separations

MDPI

Article

Simvastatin: In Vitro Metabolic Profiling of a Potent Competitive HMG-CoA Reductase Inhibitor

Wencui Yin, Reem I. Alwabli, Mohamed W. Attwa, A. F. M. Motiur Rahman * and Adnan A. Kadi *

Department of Pharmaceutical Chemistry, College of Pharmacy, King Saud University, Riyadh 11451, Saudi Arabia

* Correspondence: afmrahman@ksu.edu.sa (A.F.M.M.R.); akadi@ksu.edu.sa (A.A.K.); Tel.: +966-114670237 (A.F.M.M.R. & A.A.K.); Fax: +966-114676220 (A.F.M.M.R. & A.A.K.)

Abstract: Simvastatin (SV) is a semisynthetic derivative of lovastatin (LV), which is biosynthetically produced from the fungus *Aspergillus terreus* and has a high log *p* value (log *p* = 4.39)and thus high hepatic extraction and high efficacy in controlling cholesterol synthesis. The current study was undertaken to investigate the metabolic profile of SV using various mass spectrometry (MS) platforms. Metabolic profiling was studied in in vitro models, rat liver microsomes (RLMs), and isolated perfused rat liver hepatocytes (RLHs) using both ion trap and triple quadruple LC–MS/MS systems. A total of 29 metabolites were identified. Among them, three types of SV-related phase-I metabolites, namely exomethylene simvastatin acid (exomethylene SVA), monohydroxy SVA, and dihydrodiol SVA, were identified as new in RLMs. No phase-II metabolites were identified while incubating with RLHs.

Keywords: simvastatin; SV; SVA; RLMs; RLHs

Citation: Yin, W.; Alwabli, R.I.; Attwa, M.W.; Rahman, A.F.M.M.; Kadi, A.A. Simvastatin: In Vitro Metabolic Profiling of a Potent Competitive HMG-CoA Reductase Inhibitor. *Separations* **2022**, *9*, 400. https://doi.org/10.3390/separations9120400

Academic Editor: Isaac Rodríguez

Received: 18 October 2022
Accepted: 16 November 2022
Published: 30 November 2022

1. Introduction

The metabolism of drugs in the body (also known as biotransformation) is a complex biochemical process where drugs are structurally modified to more hydrophilic species (metabolites) enzymatically to aid in their elimination/clearance from the body [1,2]. The reactions catalyzed by drug-metabolizing enzymes can be categorized into two groups: Phase-I reactions, known as functionalization reactions and phase-II reactions, known as conjugation reactions [3]. Drug metabolism has become an integral part of drug discovery and development. The filing of an investigational new drug (IND) application of a new chemical entity (NCE) with a regulatory agency requires metabolite data derived from preclinical species to be included. Therefore, the major objectives of drug metabolism studies in development are the characterization of routes and the determination of the extent of metabolism and comparative metabolite profiling in laboratory animals of different species and humans in support of in vitro and clinical drug–drug interaction (DDI) studies and metabolites in safety testing (MIST). In the discovery phase, early metabolite identification enables medicinal chemists to chemically block or modify the major metabolic "soft spots" of the lead compound to overcome issues, such as low bioavailability, due to high first-pass metabolic clearance. A higher throughput metabolic stability screen, such as the in vitro intrinsic clearance assay using microsomes [4] or hepatocytes [5], is then performed to build a structure–metabolism relationship in addition to understanding the mechanism of disposition during lead optimization. Conducting early metabolite identification can prevent advancing a lead candidate with potential toxicity into development. In addition, the evaluation of the pharmacological activity, toxicity, and DDI potential of major metabolites in human circulation is conducted to contribute to the understanding of the safety and efficacy of the compound.

Statins, the specific and competitive inhibitors of HMG-CoA reductase (HMGR) [6], are drugs widely used for the treatment of several forms of hypercholesterolemia. They

have a potent cholesterol-lowering effect, which can arrest or reverse atherosclerosis in all vascular beds and result in a significant reduction in morbidity and mortality associated with atherosclerosis as shown by many clinical trials [7–11]. The structures of clinically significant statins usually exist in two forms, a lactone form (e.g., SV and LV) and an open-ring hydroxyl acid form (e.g., SVA, atorvastatin (AV), and pravastatin (PV)) in Figure 1 [12,13]. In the lactone form, statins are prodrugs that are readily absorbed from the gastrointestinal tract and transformed to their active forms (β-hydroxy acid) in hepatic and nonhepatic tissues [12]; on the other hand, statins in the open-ring hydroxyl acid form are active themselves as parent drugs [14]. Therefore, it is essential to perform a thorough study of their metabolism in order to understand the mechanism behind their pharmacological effects and potential side effects.

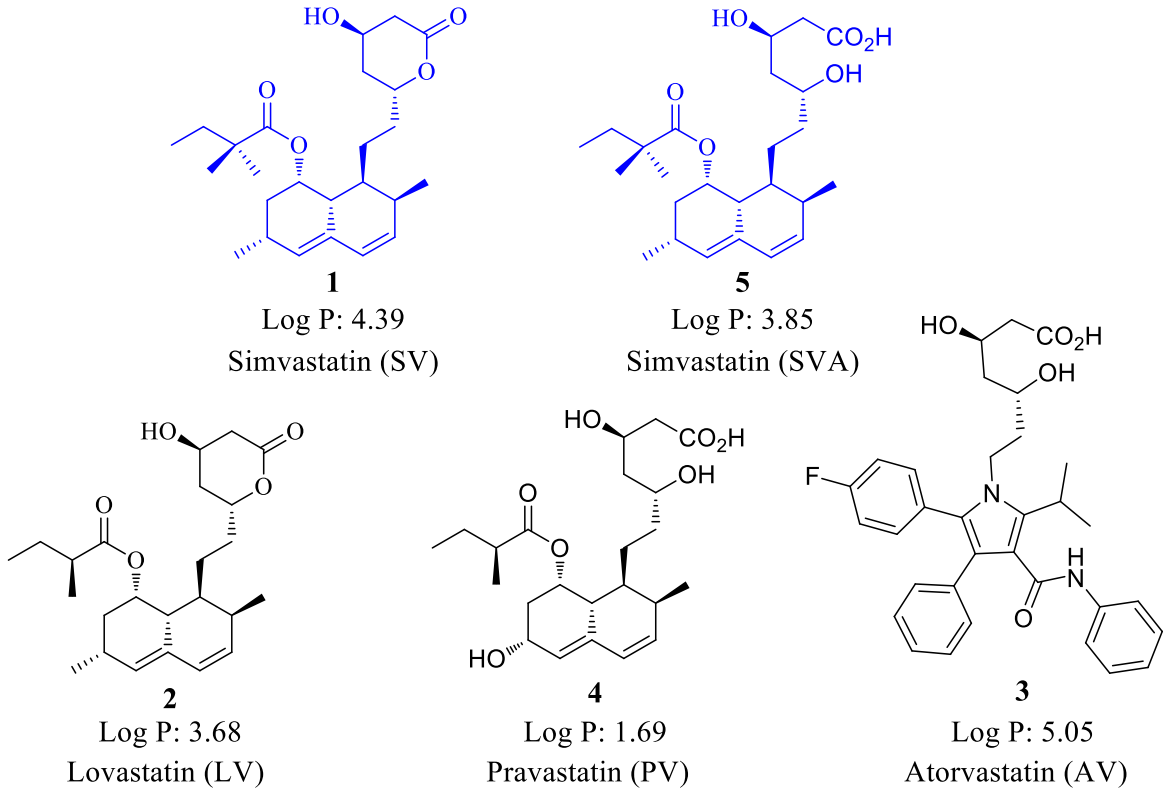

Figure 1. Chemical structures of statins and corresponding log *p* values.

SV (**1**), biosynthesized from the fungus *Aspergillus terreus* [15,16], is a semisynthetic derivative of LV (**2**). It has high hepatic extraction and high efficacy in controlling cholesterol synthesis [17], which might be due to the high log *p* value (log *p* = 4.39) of SV. SV and another cholesterol-lowering drug, AV, have been used for the clinical treatment of hypercholesterolemia worldwide [16,18]. SV has dihydroxyheptanoic acid and a ring system with lipophilic substituents. In addition, a modified hydroxyglutaric acid structurally resembles the 3-hydroxyglutaryl unit of both the substrate (HMG CoA) and the intermediate mevaldyl–CoA transition state [19], making SV a potent competitive inhibitor of HMG-CoA reductase [20]. Regardless of the effectiveness of SV in lowering cholesterol, SV has some rare and serious side effects including liver problems, muscle breakdowns, and increased blood sugar levels [21–26], in addition to common side effects including headaches, constipation, and nausea. It has also been reported that people with kidney problems should not absorb higher doses of SV [27]. It is also recommended not to take SV during pregnancy [27,28] and while breast feeding, due to the harmful effects in unborn/new-born babies. In order to maximize its excellent cholesterol-lowering effect and minimize its serious side effects, an in-depth study of its metabolism becomes indispensable to understand the mechanisms underlying its pharmacological effects and its potential side effects.

Metabolic profiling of SV has been reported in a number of articles using different analytical methods [29–33]. To date, thirteen metabolites of SV have been identified, which are depicted in Figure 2. Five metabolites **5–9** of SV were identified in rat plasma and urine using gas chromatography–mass spectrometry (GC–MS) [29]. In addition to that work, using HPLC-UV, six other metabolites **10–15** including metabolite **5** were detected in rat hepatic microsomes [30], and using NMR and mass spectroscopy [31] the same were detected in rat liver microsomes (RLMs). Later, Prueksaritanont et al. [32] identified another two new metabolites **16** and **17**, including three known metabolites **5**, **10**, and **11** using LC–MS/MS in HLMs. Moreover, Olaug S. Fenne [33] identified seven known metabolites **5** and **10–15** in HLMs by using HPLC–MS. Recently, we prepared a report about a distribution study on SV and its metabolites with a new reduced metabolite [34].

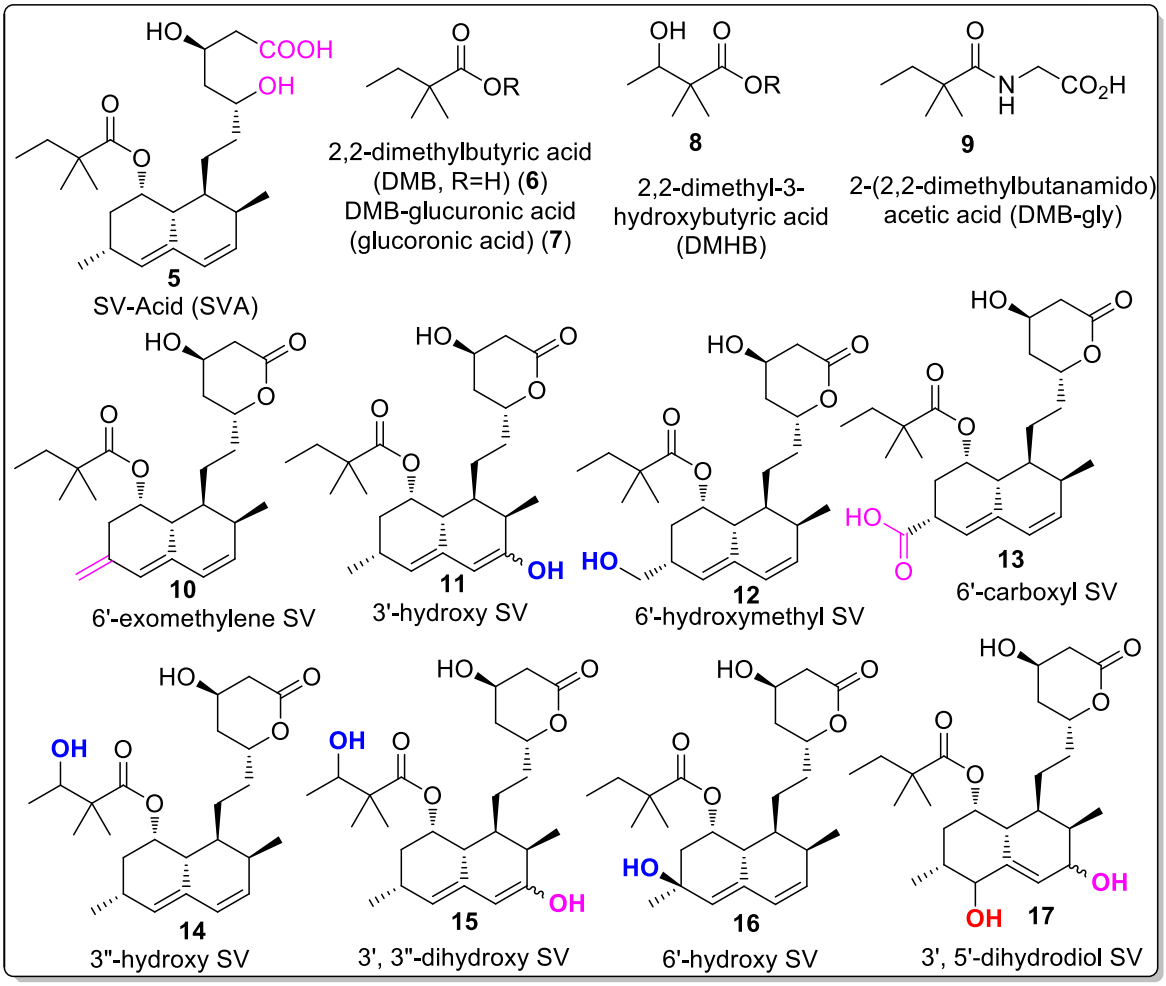

Figure 2. Reported structures of metabolites of SV (The colors indicate the possible metabolic site).

The characterization of drug-related metabolites is essential to design a new drug candidate. In this regard, high-performance liquid chromatography (HPLC) coupled with tandem mass spectrometry (MS) predominates over all other analytical tools used for screening and characterizing metabolites. MS detectors including ion trap and triple quadrupole (QqQ) have been widely used for the detection and characterization of metabolites that were generated either in vitro or in vivo due to their high selectivity and sensitivity [34–37].

In this communication, the identification and characterization of SV and its metabolites were studied in vitro in RLM and RLH incubation using ion trap and triple quadruple LC–MS/MS.

2. Materials and Methods

2.1. General

HPLC-grade water was obtained from Milli-Q and connected to Elix Millipore water purification system (Millipore, Billerica, MA, USA). Acetonitrile (ACN), HPLC-grade ammonium formate (NH_4HCO_2), ammonium acetate ($NH_4CH_3CO_2$), magnesium chloride ($MgCl_2$), and sodium hydroxide (NaOH) were obtained from BDH Laboratory Supplies, Poole, UK. Sucrose (99.7%), Ethylenebis (oxyethylenenitrilo) Tetraacetic Acid (EDTA), and Nicotinamide Adenine Dinucleotide Phosphate (NADPH) were obtained from ACROS, USA. Trypan blue, potassium chloride (KCl), potassium dihydrogen phosphate (KH_2PO_4), and sodium dihydrogen phosphate (NaH_2PO_4) were obtained from WINLAB, UK. Collagenase type 1V, HEPES (99.5%), Bovine serum albumin (BSA), and phenbarbitone were obtained from SIGMA, USA. Cupric sulfate ($CuSO_4$) and potassium sodium tartarate ($KNaC_4H_4O_6$ $4H_2O$) were obtained from PARECA QUIMICA, Spain. Sodium chloride (NaCl) and anhydrous sodium carbonate (Na_2CO_3) were obtained from AVONCHEM, UK. Magnesium sulfate ($MgSO_4$ $7H_2O$) was obtained from ALPHA CHEMIKA, India. Calcium chloride ($CaCl_2$ $2H_2O$) was obtained from Panreac, Spain. Sprague–Dawley Rats were obtained from the animal facility in the College of Pharmacy. The study was validated and approved by the committee for animal ethics of King Saud University (No. KSU-SE-19-73). SV was obtained from Sigma-Aldrich (St. Louis, MO USA), methylcellulose, distilled/deionized water, metabolic cages, oral gavage tubes, syringes, surgical tools, rotor stator homogenizer, mortar–pestle, liquid nitrogen, methanol, beakers /glass tubes/glass vials, and other equipment (i.e., −80 °C fridge, balance, centrifuge, nitrogen stream evaporator, etc.) were obtained from the lab facilities in the College of Pharmacy.

2.2. Verification of Microsomal CYP450 Activity

CYP450 activity was verified by microsomal incubation of phenytoin to produce *p*-hydroxyphenytoin [38].

2.3. Determination of Protein Content of the Prepared RLMs

Protein amount of the prepared RLMs was determined using the Lowry method [39], which is a common protein estimation assay. The UV readings based on different concentrations are listed in Table S1 and show results for the calibration curve (Figure S1). The average protein concentration of two readings of the microsomal preparations was 34.2 mg/mL.

2.4. Instrumentation

Ultracentrifugation of the liver homogenate was performed by Optima^{TM} TLX Ultracentrifuge. Measurement of protein concentrations of RLMs was performed by Variant UV spectrophotometer. Maintenance of temperature at 37 °C during rat liver hepatocyte preparation was performed by Grant (Sub Aqua Dual) water bath. Perfusion of liver was performed by Baxter (volumetric infusion pump). Agilent 1200 series LC equipped with 6320 Ion Trap/6410 QqQ mass spectrometry (Agilent Technologies, Palo Alto, CA, USA) was used for the analysis of samples.

2.5. Preparation of RLMs

2.5.1. Differential Centrifugation Method

The rat liver microsomes (RLMs) were prepared following a previously reported work [36,37,40].

2.5.2. Calcium Aggregation Method [41]

The method of Schenkman and Cinti with minor modifications was used for isolation of microsomes (Figure S2) [42].

2.5.3. Incubation of Simvastatin with Rat Liver Microsomes

Microsomal incubations were carried out according to the summary in Table S6. Aliquots of 1 mL each were used for the various types of experiments. Amounts added in each container are given in Table S6.

2.6. Isolated Perfused Rat Liver Hepatocytes

For the preparation of the isolated perfused rat hepatocytes, enzymatic method was used, in which collagenase perfusion was applied as the principle of disintegration of the liver [43].

Perfusion of Rat Liver Hepatocyte Protocol

Perfusion of rat liver hepatocytes was performed according to the previously reported work [43].

2.7. Incubation of Simvastatin with Isolated Perfused Rat Liver Hepatocytes

Incubation of SV with isolated rat hepatocytes according to the following procedure: Water bath was regularly bubbled with carbogen (95% O_2/5% CO_2) gas. The cell suspension was preincubated at 37 °C for 10 min. Hepatocyte incubations were carried out according to the summary in Table S13.

2.8. Mass Spectrometric Conditions

The column used was eclipse plus C18 (150 × 4.6 mm, 5 micron). Mobile phase composed of ammonium acetate buffer (pH = 4) in water and acetonitrile (v/v) in a gradient solvent system for 30 min (Table S2). Flow rate was 0.3 mL/min. Injection volume was 1 µL. Separation was performed on an Agilent 1200 series (Agilent Technologies, Palo Alto, CA, USA). LC–MS/MS measurements were performed using a model 6320 Ion Trap/6410 QqQ (Agilent Technologies, Palo Alto, CA, USA) equipped with an electrospray ionization source (ESI). Electrospray ionization was performed at room temperature in positive/negative modes, and the voltage was maintained at 4.5 kV and the capillary temperature at 325 °C. Scan range was set between 100 and 1000 Daltons. MS parameters were optimized for SV shown in Table S3. A direct infusion of the parent compounds (5 µg/mL) into the MS was carried out to determine the parent spectrum that served as a control spectrum for tuning the MS conditions. The infusion rate was 0.6 mL/h injection of SV on column to determine retention time for both of compounds.

3. Results and Discussion

3.1. LC–MS Data of SV

To identify SV metabolites, the chromatographic and MS fragmentation behavior of the SV was investigated as routine work. The mass spectra of SV showed the protonated molecular ion peak $[M + H]^+$ at m/z = 419 in the positive ion mode (Figure 3). Initially, the electrospray LC–MS analysis data of SV were obtained in an Agilent technologies 6320 Ion Trap LC–MS by dissolving SV in a mixture of acetonitrile (ACN) and water (H_2O) (4:1; v/v). Total ion chromatogram (TIC) showed a peak at 20.4 min (Figure 3A) with a molecular mass at m/z = 419 $[M + H]^+$, along with a sodium adduct at m/z = 441 $[M + Na]^+$ and a potassium adduct at m/z = 457 $[M + K]^+$ (Figure 3B). MS^2 spectra (Figure 3C) of SV showed several peaks including m/z = 401, 389, 383, 285, 225, 199, etc. Based on the MS^2 spectra, a fragmentation pattern of SV was proposed (Scheme 1).

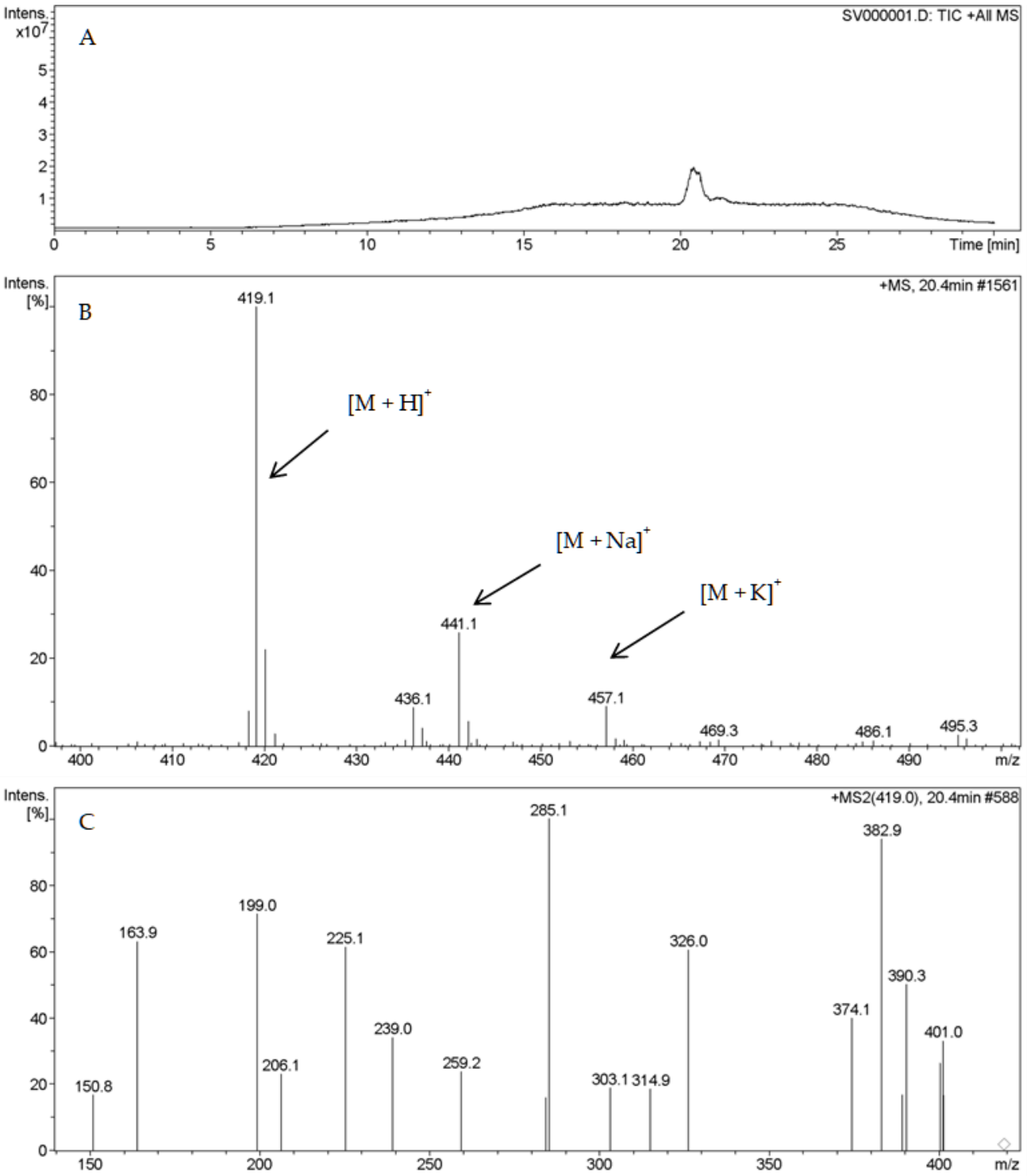

Figure 3. Total ion chromatogram (TIC) and mass spectra of SV in LC–MS positive mode: (**A**) TIC of SV; (**B**) Mass spectrum of SV; and (**C**) MS^2 spectrum of SV.

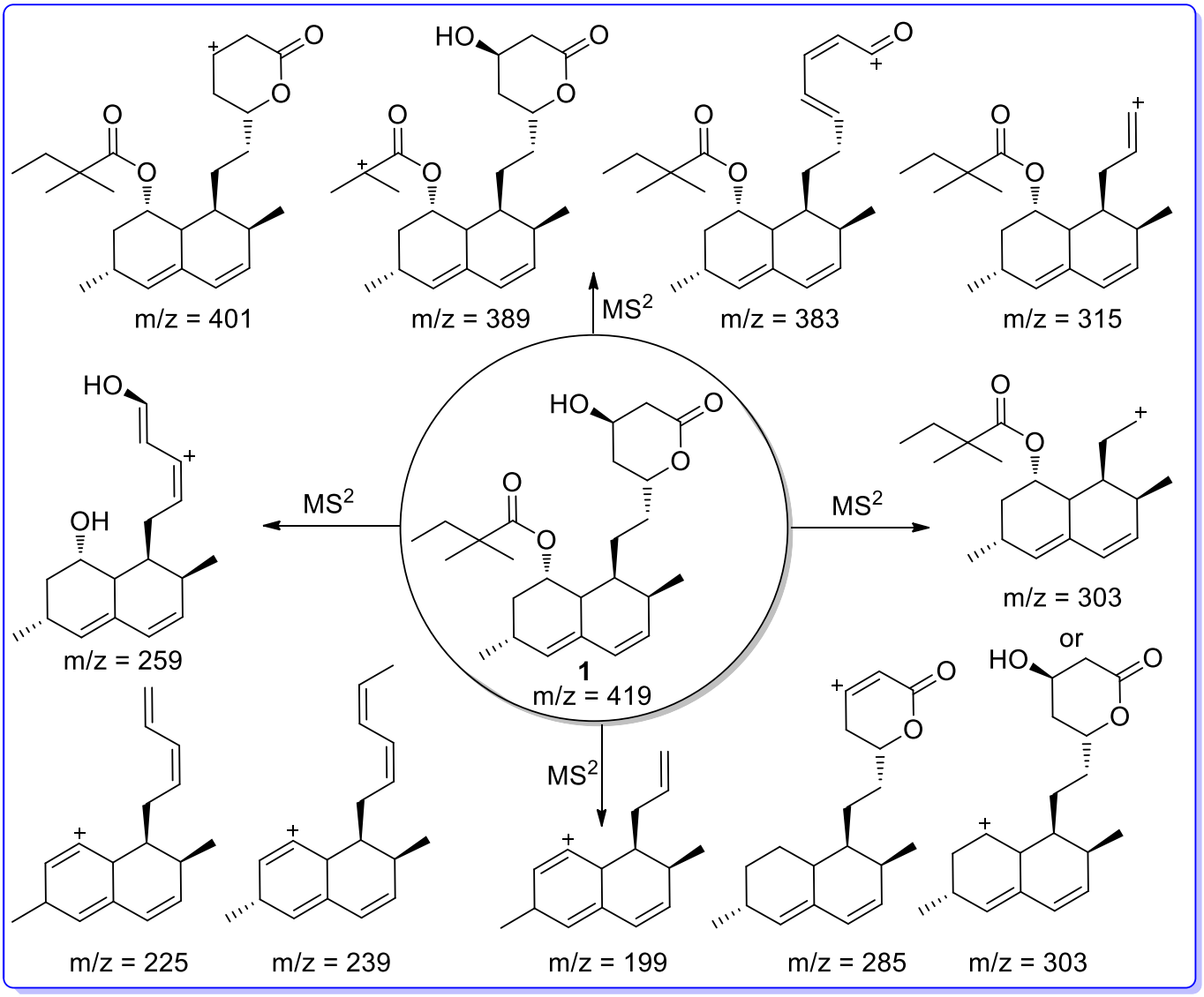

Scheme 1. Scheme shows fragmentation pattern of SV (m/z = 419 $[M + H]^+$).

3.2. Cytochrome P450-Dependent Metabolism

Screening of the TIC of SV in RLM incubation showed twenty-nine possible metabolites (Scheme 2), which might be formed by three major phase-I metabolic reactions: oxidation (hydroxylation, carboxylation, and exomethylene), reduction, and hydrolysis (SV to SVA, which was proven to be CYP-450-independent).

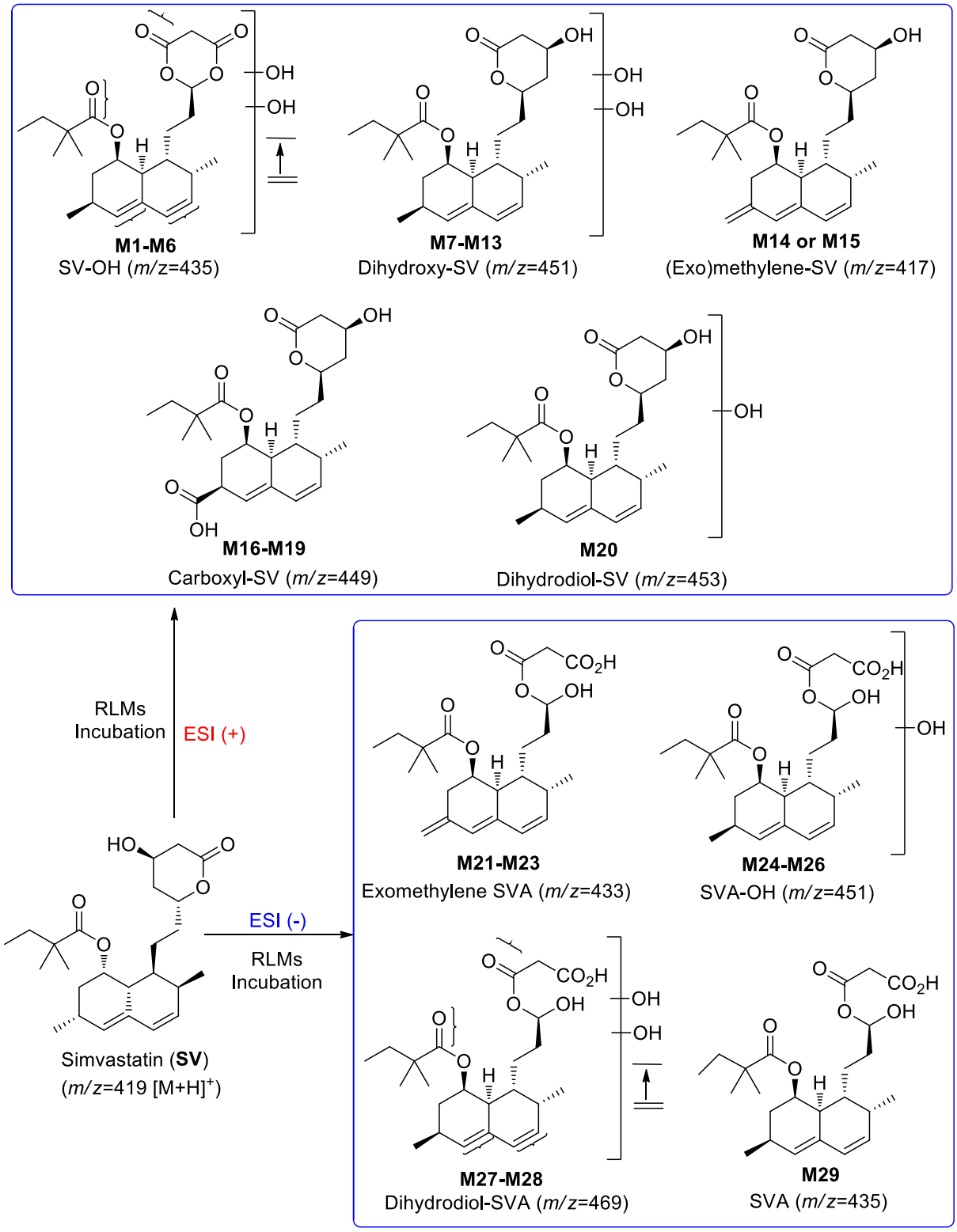

Scheme 2. Twenty-nine possible phase-I metabolites of SV.

3.3. LC–MS Data of Metabolites

3.3.1. Identification of Phase-I Metabolites

Monohydroxylated Metabolites (**M1**–**M6**)

The extracted ion chromatogram (EIC) of possible monohydroxylated metabolites (nominal mass 434 Da) at m/z = 435 revealed three peaks (Figure S4A) at the retention times

(R*ts*) of 13.4, 16.6, and 21.3 min. in the ion trap LC–MS spectrometer in the positive mode. At an R*t* of 21.3 min, a sodium adduct at m/z = 457 $[M + Na]^+$ and a potassium adduct ion at m/z = 473 $[M + K]^+$ were observed along with m/z = 435 $[M + H]^+$ (Figure S4D), whereas the other two mass spectra at R*ts* of 13.4 (Figure S4B) and 16.6 min (Figure S4C) did not reveal other adduct peaks beside m/z = 435 $[M + H]^+$. On the other front, an EIC of m/z 435 in QqQ–LC–MS in the positive mode showed six peaks (Figure S5A) compared to the above three (Figure S5A) obtained in the ion trap in the positive mode. They were at R*ts* of 12, 13.5, 14, 16.4, 17.2, and 21.2 min. Among the six peaks obtained, **M1**, **M4**, **M5**, and **M6**, appeared at retention times of 13.5 (Figure S5C), 12 (Figure S5B), 14 (Figure S5D), and 17.2 min (Figure S5F), respectively, and showed a molecular mass of m/z = 435 $[M + H]^+$ with no additional adduct ions, while **M2** at an R*t* of 16.6 min. (Figure S5E) showed a potassium adduct $[M + K]^+$ at 473 beside m/z = 435 $[M + H]^+$, and **M3** at 21.3 min. showed a molecular mass at m/z = 435 $[M + H]^+$ along with a sodium adduct $[M + Na]^+$ at m/z = 457 and a potassium adduct $[M + K]^+$ at m/z = 473 (Figure S5G). The chemical structures of six possible metabolites (Figure S6) are given in Scheme 2. The structures of the metabolites **M1**–**M6** were confirmed using the mass fragmentation pattern (Figure S7) and comparing it with the SV fragmentation pattern.

Dihydroxylated Metabolites (**M7**–**M13**)

The EIC of possible dihydroxylated metabolites (nominal mass 450 Da) at m/z = 451 showed seven peaks at R*ts* of 8.7, 9.7, 10.7, 12.6, 13.1, 15.4, and 16.9 min. in an ion trap LC–MS spectrometer (Figure S8) in the positive mode. Among them, **M7**, **M8,** and **M9** appeared at R*ts* of 8.7 (Figure S8B), 9.7 (Figure S8C), and 10.7 min. (Figure S8D), respectively, showing a molecular mass at m/z = 451 $[M + H]^+$ with no additional adduct ions, while **M10**, **M11**, **M12,** and **M13** at R*ts* of 12.6 (Figure S8E), 13.1 (Figure S8F), 15.4 (Figure S8G), and 16.9 min (Figure S8H), respectively, showed a molecular mass at m/z = 451 $[M + H]^+$ together with a sodium adduct at m/z = 473 $[M + Na]^+$ and a potassium adduct at m/z = 489 $[M + K]^+$. However, an EIC of m/z = 451 (nominal mass 450 Da) of possible dihydroxylated metabolites in QqQ–LC–MS in the positive mode yielded only three peaks at R*ts* of 9.9, 10.2 and 11.2 min (Figure S9), which seemed to be corresponding to **M7**, **M8,** and **M9** detected in the ion trap LC–MS spectrometer. The EIC and the mass spectra of those possible metabolites are given in Figure S9. The chemical structures of seven possible metabolites (Figure S10) are given in Scheme 2. The structures of the metabolites **M7–M13** were confirmed using the mass fragmentation pattern (Figure S11) and comparing it with the SV fragmentation pattern.

Exomethylene SV (**M14** and/or **M15**)

A possible oxidized metabolite (exomethylene SV) **M14** and/or **M15** at an R*t* of 16.2 min. was observed when the EIC of m/z = 417 (nominal mass 416 Da) was performed in an ion trap–MS in the positive mode (Figure S12A). The mass spectrum at an R*t* of 16.2 min. (Figure S12B) showed m/z = 417 $[M + H]^+$ with a sodium adduct at 439 $[M + Na]^+$ and a potassium adduct at m/z = 455 $[M + K]^+$. In contrast, an EIC of m/z = 417 in QqQ–LC–MS in the positive mode generated two peaks (Figure S13A) at 15.3 and 21.3 min., where the protonated ion peaks at m/z = 417 $[M + H]^+$ were displayed with no adduct ions (Figure S13B,C). The chemical structures of the possible exomethylene SV (Figure S14) are demonstrated in Scheme 2.

Carboxyl-SV (**M16**–**M19**)

Four possible oxidized metabolites (carboxyl-SV) **M16**–**M19** at R*ts* of 14.1, 14.8, 15.5 and 16.9 min., respectively, were observed at an EIC of m/z = 449 (nominal mass 448 Da) in the ion trap–MS in the positive mode. All the peaks appeared along with adduct ions (Figure S15). All the mass spectra showed a m/z = 449 $[M + H]^+$ with a sodium adduct at 471 $[M + Na]^+$ and a potassium adduct at m/z = 487 $[M + K]^+$, while in QqQ–LC–MS in the positive mode, three peaks were observed at R*ts* of 13.0, 14.1, and 16.9 min. Among

them, two peaks (at R*ts* of 14.1 and 16.9 min. appeared along with the adduct ions (Figure S16) m/z = 449 $[M + H]^+$ with a sodium adduct at 471 $[M + Na]^+$ and a potassium adduct at m/z = 487 $[M + K]^+$. The chemical structures of the four possible oxidized (carboxyl-SV) metabolites (Figure S17) are displayed in Scheme 2. The structures of the metabolites **M16**–**M19** were confirmed using the mass fragmentation pattern (Figure S18) and comparing it with the SV fragmentation pattern.

Dihydrodiol Metabolite (**M20**)

A possible dihydrodiol metabolite **M20** was only observed at an EIC of m/z = 453 (nominal mass 452 Da) in a QqQ–LC–MS in the positive mode at an R*t* of 12.0 min. (Figure S19) which showed m/z = 453 $[M + H]^+$. The chemical structures of the possible dihydrodiol metabolites (Figure S20) are displayed in Scheme 2.

Exomethylene-SVA Metabolites (**M21**–**M23**)

Here, three possible exomethylene-SVA metabolites **M21**–**M23** were observed at an EIC of m/z = 433 (nominal mass 434 Da) in the negative mode (Figure S21). **M21** was identified at an R*t* of 21.8 min in ion trap–MS, and **M22** and **M23** were identified at 11.1 min. and 13.3 min., respectively, in QqQ–LC–MS. All the peaks showed m/z = 433 $[M + H]^-$. The chemical structures of the possible exomethylene SVA metabolites (Figure S22) are given in Scheme 2.

Hydroxl-SVA Metabolites (**M24**–**M26**)

Three possible hydroxyl-SVA metabolites **M24**–**M26** were observed at an EIC of m/z = 451 (nominal mass 452 Da) and at an R*t* of 13.3 min. in an ion trap–MS in the negative mode, which showed m/z = 451 $[M + H]^-$, and R*ts* of 6.2 and 6.9 min. in QqQ–MS in the negative mode, which also showed m/z = 451 $[M + H]^-$ (Figure S23). The chemical structures of the possible hydroxyl-SVA metabolites (Figure S24) are given in Scheme 2.

Dihydrodiol-SVA Metabolites (**M27**–**M28**)

Two possible dihydrodiol-SVA metabolites **M27** and **M28** were observed (Figure S25) at an EIC of m/z = 469 (nominal mass 470 Da) and at an R*t* of 8.1 min. in ion trap–MS in the negative mode (Figure S25A) and 4.9 min. in QqQ–C–MS in the negative mode. Both showed m/z = 469 $[M + H]^-$ (Figure S25B). The chemical structures of the possible dihydrodiol-SVA metabolites (Figure S26) are given in Scheme 2.

Hydrolyzed-SV (SVA) Metabolites (**M29**)

Hydrolyzed-SV (SVA) metabolite **M29** at a R*t* of 22.9 min. (Figure S27A) in ion trap–MS was observed at an EIC of m/z = 435 (nominal mass 436 Da). The mass spectrum of **M29** showed m/z = 435 $[M + H]^-$ in the negative mode (Figure S27C). The same peak was also observed in the control while incubated without NADPH (Figure S27B) with m/z = 435.1. This peak also showed m/z = 435 $[M + H]^-$ (Figure S27D). No peaks were observed in absence of either SV or RLMs. The structures of the metabolites **M29** were confirmed using the mass fragmentation pattern (Figure S28) and comparing it with the SV fragmentation pattern. The conversion of SV to SVA was previously reported [44] claiming independence of NADPH in the reversible conversion of SV to SVA, which is catalyzed by esterases, not by CYP 450 reactions [44]. SV is hydrolyzed to its active metabolite simvastatin acid (SVA) by esterase after oral absorption. Among all the esterases, carboxylesterase (CES) and paraoxonase (PON) were reported to be involved in the conversion of SV to SVA in human blood. CES was found to be the major esterase that activated SV in rat blood, while PON showed almost no hydrolysis effect toward SV. In addition, the rate of converting SV to SVA is much lower in human plasma than in rat plasma. The CES was found mostly expressed in the liver and has been detected in the blood, small intestine, kidneys, and lungs in humans/rats. CES1 has only been detected in human blood, while both CES1 and CES2 have been found in rat blood. In the meantime, PON1 was highly expressed in the

liver and then secreted into the blood followed by PON3 in both humans and rats. The expression levels and substrate specificities of CES and PON exhibited differences between humans and rats, implying that the esterase-mediated hydrolysis of SV in rats and humans could be different [45]. Therefore, the metabolic profiling of SV collected in rats might not be able to fully represent the metabolic profiling of SV in humans, leading to the necessity of further clinical trials. Rat microsomal esterase (hydrolytic reaction) is shown below (Scheme 3), which is not a CYP450-involved reaction, and is thus NADPH-independent.

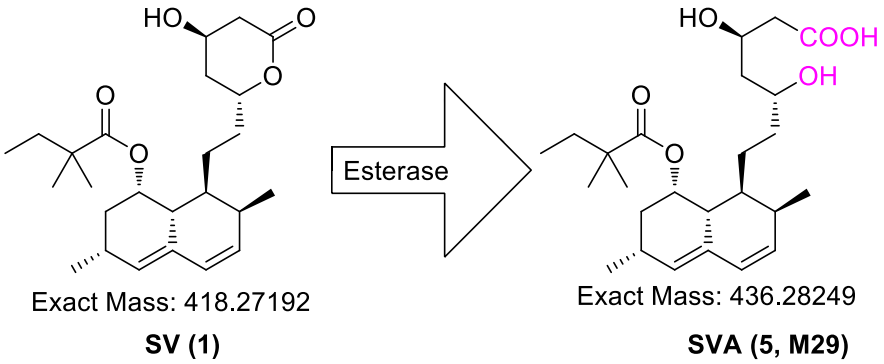

Scheme 3. Structure of possible SVA metabolites (**M29**) (Purple color indicate the possible metabolic site).

No metabolites were detected in the absence of SV, NADPH, or RLMs except **M29** in the absence of NADPH.

Summary of Detected Phase-I Metabolites in LC–MS

Twenty metabolites, which were identified in the positive mode in ion trap/QqQ MS, are summarized in Table 1 with their R*t* values.

Table 1. Simvastatin metabolites identified in ion trap/QqQ MS in positive mode.

Detected Metabolites	No.	Ion Trap		QqQ		ESI (+) (*m*/*z*)
		R*t* (min)	Detected	R*t* (min)	Detected	
Monohydroxy-SV	**M1**	13.4	√	13.5	√	435
	M2	16.6	√	16.4	√	
	M3	21.3	√	21.2	√	
	M4	-	-	12	√	
	M5	-	-	14	√	
	M6	-	-	17.2	√	
Dihydroxy-SV	**M7**	8.7.	√	9.9	√	451
	M8	9.7	√	10.2	√	
	M9	10.7	√	11.2	√	
	M10	12.6	√	-	-	
	M11	13.1	√	-	-	
	M12	15.4	√	-	-	
	M13	16.9	√	-	-	
Exomethylene-SV	**M14**	16.2	√	15.3	√	417
	M15	-	-	21.3	√	
Carboxyl-SV	**M16**	14.1	√	13	√	449
	M17	14.8	√	14	√	
	M18	15.5	√	-	-	
	M19	16.9	√	16.7	√	
Dihydrodiol-SV	**M20**	-	-	12	√	453

Nine metabolites, which were identified in the negative mode in ion trap/QqQ MS, are summarized in Table 2 with their R*t* values.

Table 2. Simvastatin metabolites detected in QqQ/ion trap–MS in negative mode.

Detected Metabolites	No.	Ion Trap		QqQ		ESI (−) (*m*/*z*)
		Rt (min)	Detected	Rt (min)	Detected	
Exomethylene-SVA	**M21**	21.8	√	-	-	433
	M22	-	-	11.1	√	
	M23	-	-	13.3	√	
Monohydroxy-SVA	**M24**	13.3	√	-	-	451
	M25	-	-	6.2	√	
	M26	-	-	6.9	√	
Dihydrodiol-SVA	**M27**	8.1	√	-	-	469
	M28	-	-	4.9	√	
SVA	**M29**	22.9	√	-	-	435

All the above mentioned phase-I metabolic reactions, which led to the generation of different phase-I metabolites, were set in parallel with three controls (Table S6): incubations in the absence of SV, NADPH, and RLMs. The samples were properly prepared before being directed into both LC–ion trap–MS and LC–QqQ–MS for analysis. The results prove the indispensible involvement of CYP450, which is NADPH-dependent, in all the tested common metabolic reactions of SV, except for the reversible conversion of SV to its active SVA. The same peaks observed in LC–ion trap–MS in the negative mode at an EIC of 435 generated from the samples with/without NADPH (Figure S27B,D) confirmed the previously reported NADPH independence [46] in the conversion of SV lactone to the active hydroxy acid form. No peaks were observed in LC–ion Trap–MS in the negative mode at an EIC of 435 generated from the sample in the absence of RLM, indicating the invovlement of the enzyme esterase [46,47] in the hydrolysis of SV lactone to the active hydroxy acid form SVA, which ruled out its possiblitity of being a nonenzymatic process.

The identified possible SV metabolites in the rat in vitro experiment were in accordance with previously reported SV metabolites [29–33]. In addition, we detected some possible SVA metabolites in this experiment (Section 3.3.1), which, to the best of our knowledge, have beeen reported only once in a paper, where SVA was used as a substrate instead of SV to identify the responsiblility of CYP450 isoforms for the metabolism of SVA in human liver microsomes (HLMs) [48].

3.3.2. Identification of Phase-II Metabolites

Possible phase-II cojugation reactions of SV and SV acid are illustrated in Scheme 4. Phase-II cojugation reactions happen if the groups -OH, -CO_2H, -NH(R), and -SH are present in a molecule. Phase-II reactions include glucuronidation, glutathion conjugation, sulfation, methylation, acylation, and amino acid conjugation. However, no phase-II metabolites were identified either in ion trap–and/or QqQ–mass spectrometry. On the one hand, high levels of easterase reside in rat plasma resulting in rapid hydrolysis of SV into SVA [46,47], which might be the reason behind the failure to observe phase-II metabolites of SV. On the other hand, SVA was reported to undergo glucuronidation with the presence of UGTs (also called glucuronyltransferase) and its cofactor uridine diphosphoglucuronic acid (UDPGA) (available in hepatocytes, where a complete set of enzyme systems as well as cofactors are coexisting) [49] to form SVA glucuronide, which was so far reported only in the bile collected from a dog after intravenous (IV) administration of [^{14}C] SVA. In addition, upon studying the stability of the formed SVA glucuronide, it was found to be quite unstable and susceptible to spontaneous cyclization/laconization to SV upon isolation from in vitro incubation. The rate of glucuronide-to-lactone conversion was even higher under conditions of a physiological pH (pH 7–8) range [50]. Thus, the relative ease of spontaneous cyclization of the SVA glucuronide, which contributes partially to the mechanism of SV formation, may explain the reduced tendency and its failure to detect phase-II metabolites of SVA in our study.

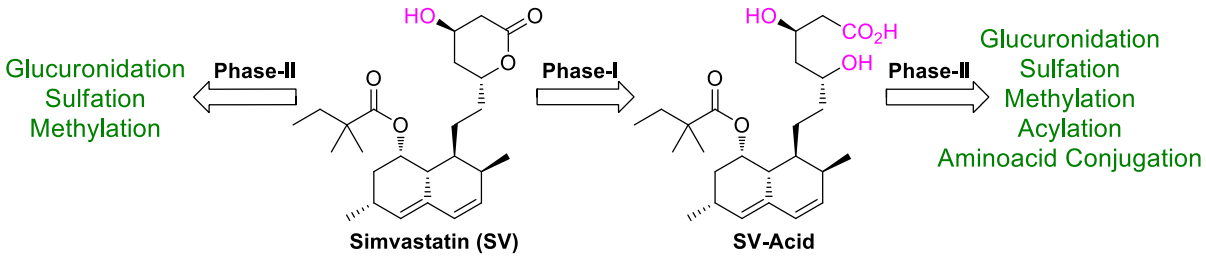

Scheme 4. Possible phase-II cojugation reactions of SV and SV acid.

4. Conclusions

In vitro metabolic profiling of SV in RLMs using both LC–Ion Trap–MS and LC–QqQ–MS revealed three types of new SV-related metabolites in RLMs; they are exomethylene-SVA, monohydroxy-SVA and dihydrodiol-SVA, adding a more complete picture to the previously reported metabolic profiling of simvastatin, which will, we believe, provide crucial data on these new metabolites for possible later study of DDIs associated with metabolism. While attempting to discover more complete metabolic profiling, we compared both LC–ion trap–MS vs. LC–QqQ–MS and found that the former outperformed the latter in metabolite identification in our study, which agrees with the former being a better choice for the quantitative analysis than the latter. No phase-II metabolites were identified while incubating SV in RLHs; this might be due to the spontaneous cyclization of the SVA glucuronide, which contributes partially to the mechanism of SV formation.

Supplementary Materials: The following supporting information can be downloaded at: https://www.mdpi.com/article/10.3390/separations9120400/s1, Figure S1: Schematic representation of RLMs preparation step; Figure S2: Calibration curve of different standard of protein concentration; Figure S3: Calibration curve of different standard of protein concentration; Figure S4: Mass Spectra of **M1**–**M3** in Ion Trap; Figure S5: Mass Spectra of **M1**–**M6** in QqQ; Figure S6: Possible structures of **M1**–**M6**; Figure S7: MS^2 spectra of **M1**–**M6**; Figure S8: Mass Spectra of **M7**–**M13** in Ion Trap; Figure S9: Mass Spectra of **M7**–**M9** in QqQ; Figure S10: Possible structures of **M7**–**M13**; Figure S11: MS2 spectra of **M7**–**M13**; Figure S12: Mass Spectra of **M14** or **M15** in Ion Trap; Figure S13: Mass Spectra of **M14** or **M15** in QqQ; Figure S14: Possible structures of **M14** or **M15**; Figure S15: Mass Spectra of **M16**–**M19** in Ion Trap; Figure S16: Mass Spectra of **M16**–**M19** in QqQ; Figure S17: Possible structures of **M16**–**M19**; Figure S18: MS^2 spectra of **M16**–**M19**; Figure S19: Mass Spectra of **M20** in QqQ; Figure S20: Possible structures of **M20**; Figure S21: Mass Spectra of **M21**–**M23** in Ion Trap/QqQ; Figure S22: Possible structures of **M21**–**M23**; Figure S23: Mass Spectra of **M24**–**M26** in Ion Trap/QqQ; Figure S24: Possible structures of **M24**–**M26**; Figure S25: Mass Spectra of **M27**–**M28** in Ion Trap/QqQ; Figure S26: Possible structures of **M27**–**M28**; Figure S27: Mass Spectra of **M29** in Ion Trap; Figure S28: MS2 spectra of **M29**; Table S1: Concentration of Protein (Calibration curve of BSA); Table S2: RLMs Incubations; Table S3: RLMs Incubations; Table S4: Gradient solvent system used in HPLC separation of microsomal incubations; Table S5: Optimized MS parameters for SV. References [51,52] are cited in the Supplementary Materials.

Author Contributions: Methodology and Data collection, W.Y.; Supervision, Data collection, Investigation, Writing—original draft, and Writing—review and editing, A.F.M.M.R.; Writing—review and editing, M.W.A.; Supervision and Writing—review and editing, R.I.A.; Supervision, Writing—review and editing, and Funding acquisition, A.A.K. All authors have read and agreed to the published version of the manuscript.

Funding: This research was funded by Deanship of Scientific Research at King Saud University, Research Group Project No. RG-1437-033.

Institutional Review Board Statement: The study was validated and approved by the committee for animal ethics of King Saud University (No. KSU-SE-19-73 dated on 18 March 2019).

Data Availability Statement: All the experimental data are available in the supporting file as well authors on request.

Acknowledgments: The authors would like to extend their sincere appreciation to the Deanship of Scientific Research at King Saud University for funding this work through the Research Group Project No. RG-1437-033.

Conflicts of Interest: The authors declare no conflict of interest.

References

1. Wen, B.; Zhu, M. Applications of mass spectrometry in drug metabolism: 50 years of progress. *Drug Metab. Rev.* **2015**, *47*, 71–87. [CrossRef] [PubMed]
2. Zhang, Z.; Tang, W. Drug metabolism in drug discovery and development. *Acta Pharm. Sin. B* **2018**, *8*, 721–732. [CrossRef] [PubMed]
3. Wen, B.; Nelson, S.D. Common Biotransformation Reactions. In *Mass Spectrometry in Drug Metabolism and Disposition: Basic Principles and Applications*, 1st ed.; Lee, M.S., Zhu, M., Eds.; John Wiley & Sons, Inc: Hoboken, NJ, USA, 2011; pp. 13–41.
4. Obach, R.S. Prediction of human clearance of twenty-nine drugs from hepatic microsomal intrinsic clearance data: An examination of in vitro half-life approach and nonspecific binding to microsomes. *Drug Metab. Dispos.* **1999**, *27*, 1350–1359. [PubMed]
5. Carlile, D.J.; Stevens, A.J.; Ashforth, E.I.; Waghela, D.; Houston, J.B. In vivo clearance of ethoxycoumarin and its prediction from In vitro systems. Use Of drug depletion and metabolite formation methods in hepatic microsomes and isolated hepatocytes. *Drug Metab. Dispos.* **1998**, *26*, 216–221.
6. Endo, A.; Kuroda, M.; Tanzawa, K. Competitive inhibition of 3-hydroxy-3-methylglutaryl coenzyme A reductase by ML-236A and ML-236B fungal metabolites, having hypocholesterolemic activity. *FEBS Lett.* **1976**, *72*, 323–326. [CrossRef]
7. Nováková, L.; Vlčková, H.; Šatínský, D.; Sadílek, P.; Solichová, D.; Bláha, M.; Bláha, V.; Solich, P. Ultra-high-performance liquid chromatography tandem mass spectrometric detection in clinical analysis of simvastatin and atorvastatin. *J. Chromatogr. B* **2009**, *877*, 2093–2103. [CrossRef]
8. Shitara, Y.; Sugiyama, Y. Pharmacokinetic and pharmacodynamic alterations of 3-hydroxy-3-methylglutaryl coenzyme A (HMG-CoA) reductase inhibitors: Drug–drug interactions and interindividual differences in transporter and metabolic enzyme functions. *Pharmacol. Ther.* **2006**, *112*, 71–105. [CrossRef]
9. Sandhu, S.; Wiebe, N.; Fried, L.F.; Tonelli, M. Statins for improving renal outcomes: A meta-analysis. *J. Am. Soc. Nephrol.* **2006**, *17*, 2006–2016. [CrossRef]
10. Sacks, F.M. The relative role of low-density lipoprotein cholesterol and high-density lipoprotein cholesterol in coronary artery disease: Evidence from large-scale statin and fibrate trials. *Am. J. Cardiol.* **2001**, *88*, 14–18. [CrossRef]
11. Bertolini, S.; Bittolo Bon, G.; Campbell, L.M.; Farnier, M.; Langan, J.; Mahla, G.; Pauciullo, P.; Sirtori, C.; Egros, F.; Fayyad, R.; et al. Efficacy and safety of atorvastatin compared to pravastatin in patients with hypercholesterolemia. *Atherosclerosis* **1997**, *130*, 191–197. [CrossRef]
12. Yang, D.J.; Hwang, L.S. Study on the conversion of three natural statins from lactone forms to their corresponding hydroxy acid forms and their determination in Pu-Erh tea. *J. Chromatogr. A* **2006**, *30*, 277–284. [CrossRef] [PubMed]
13. Jemal, M.; Xia, Y.Q. Bioanalytical method validation design for the simultaneous quantitation of analytes that may undergo interconversion during analysis. *J. Pharm. Biomed. Anal.* **2000**, *22*, 813–827. [CrossRef] [PubMed]
14. Corsini, A.; Maggi, F.M.; Catapano, A.L. Pharmacology of competitive inhibitors of HMG-CoA reductase. *Pharmacol. Res.* **1995**, *31*, 9–27. [CrossRef]
15. Pawan Kumar, B.; Deepti, J. Simvastatin: Review of Updates on Recent Trends in Pharmacokinetics, Pharmacodynamics, Drug–drug Interaction, Impurities and Analytical Methods. *Curr. Pharm. Anal.* **2012**, *8*, 135–156. [CrossRef]
16. Simvastatin. Available online: http://www.drugs.com/monograph/simvastatin.html (accessed on 20 June 2022).
17. Alberts, A.W. Lovastatin and simvastatin—Inhibitors of HMG CoA reductase and cholesterol biosynthesis. *Cardiology* **1990**, *77* (Suppl. 4), 14–21. [CrossRef]
18. Bybee, K.A.; Lee, J.H.; O'Keefe, J.H. Cumulative clinical trial data on atorvastatin for reducing cardiovascular events: The clinical impact of atorvastatin. *Curr. Med. Res. Opin.* **2008**, *24*, 1217–1229. [CrossRef] [PubMed]
19. Roche, V.F. Antihyperlipidemic Statins: A Self-Contained, Clinically Relevant Medicinal Chemistry Lesson. *Am. J. Pharm. Educ.* **2005**, *69*, 77. [CrossRef]
20. Lennernäs, H.; Fager, G. Pharmacodynamics and pharmacokinetics of the HMG-CoA reductase inhibitors. Similarities and differences. *Clin. Pharmacokinet.* **1997**, *32*, 403–425. [CrossRef]
21. Naci, H.; Brugts, J.; Ades, T. Comparative tolerability and harms of individual statins: A study-level network meta-analysis of 246,955 participants from 135 randomized, controlled trials. *Circ. Cardiovasc. Qual. Outcomes* **2013**, *6*, 390–399. [CrossRef]
22. Di Stasi, S.L.; MacLeod, T.D.; Winters, J.D.; Binder-Macleod, S.A. Effects of statins on skeletal muscle: A perspective for physical therapists. *Phys. Ther.* **2010**, *90*, 1530–1542. [CrossRef]
23. Alkhatatbeh, M.J.; Abdul-Razzak, K.K.; Khasawneh, L.Q.; Saadeh, N.A. Prevalence of musculoskeletal pain in association with serum 25-hydroxyvitamin D concentrations in patients with type 2 diabetes mellitus. *Biomed. Rep.* **2018**, *8*, 571–577. [CrossRef] [PubMed]
24. Weise, W.J.; Possidente, C.J. Fatal rhabdomyolysis associated with simvastatin in a renal transplant patient. *Am. J. Med.* **2000**, *108*, 351–352. [CrossRef] [PubMed]

25. Summaries for Patients. Muscle abnormalities in four patients taking statins to treat unfavorable cholesterol levels. *Ann. Intern. Med.* **2002**, *137*, I45. [CrossRef] [PubMed]
26. Meier, C.R.; Schlienger, R.G.; Kraenzlin, M.E.; Schlegel, B.; Jick, H. HMG-CoA reductase inhibitors and the risk of fractures. *JAMA* **2000**, *283*, 3205–3210. [CrossRef] [PubMed]
27. Pommier, Y. DNA topoisomerase I inhibitors: Chemistry, biology, and interfacial inhibition. *Chem. Rev.* **2009**, *109*, 2894–2902. [CrossRef] [PubMed]
28. Prescribing Medicines in Pregnancy Database. Available online: https://www.huidziekten.nl/formularium/documenten/medicines-pregnancy.pdf (accessed on 20 June 2022).
29. Uchiyama, N.; Kagami, Y.; Saito, Y.; Abe, S.; Ohtawa, M.; Hata, S. Metabolic fate of 2,2-dimethylbutyryl moiety of simvastatin in rats: Identification of metabolites by gas chromatography/ mass spectrometry. *Eur. J. Drug Metab. Pharmacokinet.* **1991**, *16*, 189–196. [CrossRef] [PubMed]
30. Ohtawa, M.; Uchiyama, N. Sex difference in metabolism of simvastatin by rat hepatic microsomes. *Eur. J. Drug Metab. Pharmacokinet.* **1992**, *17*, 175–181. [CrossRef]
31. Uchiyama, N.; Kagami, Y.; Saitoh, Y.; Ohtawa, M. Male-specific metabolism of simvastatin by rat liver microsomes. *Chem. Pharm. Bull.* **1991**, *39*, 236–238. [CrossRef]
32. Prueksaritanont, T.; Gorham, L.M.; Ma, B.; Liu, L.; Yu, X.; Zhao, J.J.; Slaughter, D.E.; Arison, B.H.; Vyas, K.P. In vitro metabolism of simvastatin in humans [SBT] identification of metabolizing enzymes and effect of the drug on hepatic P450s. *Drug Metab. Dispos.* **1997**, *25*, 1191–1199.
33. Fenne, O.S. In Vitro Studies Suggest Involvement of CYP2D6 in the Metabolism of Simvastatin and Active Metabolites. Master's Thesis, University of Oslo, Oslo, Norway, 2003.
34. Yin, W.; Al-Wabli, R.I.; Attwa, M.W.; Rahman, A.F.M.M.; Kadi, A.A. Detection and characterization of simvastatin and its metabolites in rat tissues and biological fluids using MALDI high resolution mass spectrometry approach. *Sci. Rep.* **2022**, *12*, 4757. [CrossRef]
35. Kadi, A.A.; Yin, W.; Rahman, A.F.M.M. In-Vitro metabolic profiling study of potential topoisomerase inhibitors 'pyrazolines' in RLMs by mass spectrometry. *J. Chromatogr. B* **2019**, *1114*, 125–133. [CrossRef] [PubMed]
36. Rahman, A.F.M.M.; Al-Shakliah, N.S.; Yin, W.; Kadi, A.A. In vitro Investigation of Metabolic Profiling of a Potent Topoisomerase Inhibitors Fluorescein Hydrazones (FLHs) in RLMs by LC-MS/MS. *J. Chromatogr. B* **2017**, *1054*, 27–35. [CrossRef] [PubMed]
37. Kadi, A.A.; Al-Shakliah, N.S.; Yin, W.; Rahman, A.F.M.M. In vitro investigation of metabolic profiling of newly developed topoisomerase inhibitors (ethyl fluorescein hydrazones, EtFLHs) in RLMs by LC–MS/MS. *J. Chromatogr. B* **2017**, *1054*, 93–104. [CrossRef] [PubMed]
38. Billings, R.E. Sex differences in rats in the metabolism of phenytoin to 5-(3,4-dihydroxyphenyl)-5-phenylhydantoin. *J. Pharmacol. Exp. Ther.* **1983**, *225*, 630–636. [PubMed]
39. Lowry, O.H.; Rosebrough, N.J.; Farr, A.L.; Randall, R.J. Protein measurement with the Folin phenol reagent. *J. Biol. Chem.* **1951**, *193*, 265–275. [CrossRef]
40. Mountney, A.; Boutte, A.M.; Gilsdorf, J.; Lu, X.C.; Tortella, F.C.; Shear, D.A. Intravenous Administration of Simvastatin Improves Cognitive Outcome following Severe Traumatic Brain Injury in Rats. *J. Neurotrauma* **2016**, *33*, 1492–1500. [CrossRef]
41. Iyer, K.; Walawalkar, P.; Serai, P. Isolation and catalytic competence of different animal liver microsomal fractions prepared by calcium-aggregation method. *Indian J. Pharm. Sci.* **2006**, *2*, 262. [CrossRef]
42. Schenkman, J.B.; Cinti, D.L. Preparation of microsomes with calcium. *Methods Enzymol.* **1978**, *52*, 83–89.
43. Berry, M.N.; Friend, D.S. High-yield preparation of isolated rat liver parenchymal cells: A biochemical and fine structural study. *J. Cell Biol.* **1969**, *43*, 506–520. [CrossRef]
44. Germershausen, J.I.; Hunt, V.M.; Bostedor, R.G.; Bailey, P.J.; Karkas, J.D.; Alberts, A.W. Tissue selectivity of the cholesterol-lowering agents lovastatin, simvastatin and pravastatin in rats in vivo. *Biochem. Biophys. Res. Commun.* **1989**, *158*, 667–675. [CrossRef]
45. Li, Z.; Zhang, J.; Zhang, Y.; Zuo, Z. Role of esterase mediated hydrolysis of simvastatin in human and rat blood and its impact on pharmacokinetic profiles of simvastatin and its active metabolite in rat. *J. Pharm. Biomed. Anal.* **2019**, *168*, 13–22. [CrossRef] [PubMed]
46. Vickers, S.; Duncan, C.A.; Vyas, K.P.; Kari, P.H.; Arison, B.; Prakash, S.R.; Ramjit, H.G.; Pitzenberger, S.M.; Stokker, G.; Duggan, D.E. In vitro and in vivo biotransformation of simvastatin, an inhibitor of HMG CoA reductase. *Drug Metab. Dispos.* **1990**, *18*, 476–483. [PubMed]
47. Vickers, S.; Duncan, C.A.; Chen, I.W.; Rosegay, A.; Duggan, D.E. Metabolic disposition studies on simvastatin, a cholesterol-lowering prodrug. *Drug Metab. Dispos.* **1990**, *18*, 138–145.
48. Prueksaritanont, T.; Ma, B.; Yu, N. The human hepatic metabolism of simvastatin hydroxy acid is mediated primarily by CYP3A, and not CYP2D6. *Br. J. Clin. Pharmacol.* **2003**, *56*, 120–124. [CrossRef] [PubMed]
49. Zhang, D.; Luo, G.; Ding, X.; Lu, C. Preclinical experimental models of drug metabolism and disposition in drug discovery and development. *Acta Pharm. Sin. B* **2012**, *2*, 549–561. [CrossRef]
50. Prueksaritanont, T.; Subramanian, R.; Fang, X.; Ma, B.; Qiu, Y.; Lin, J.H.; Pearson, P.G.; Baillie, T.A. Glucuronidation of Statins in Animals and Humans: A Novel Mechanism of Statin Lactonization. *Drug Metab. Dispos.* **2002**, *30*, 505–512. [CrossRef]
51. Fish, R.; Danneman, P.; Brown, M.; Karas, A. *Anesthesia and Analgesia in Laboratory Animals*; Academic Press: London, UK, 1997.
52. Strober, W. Trypan blue exclusion test of cell viability. *Curr. Protoc. Immunol.* **2001**, *3*, A3B1–A3B2.